Deterministic generation of large-scale hyperentanglement in three degrees of freedom

Xutong Wang[a], Sheng Yu[a], Shengshuai Liu[a], Kai Zhang[a], Yanbo Lou[a], Wei Wang[a], Jietai Jing[a,b,c,d,*]

[a]East China Normal University, School of Physics and Electronic Science, Joint Institute of Advanced Science and Technology, State Key Laboratory of Precision Spectroscopy, Shanghai, China, 200062
[b]CAS Center for Excellence in Ultra-intense Laser Science, Shanghai, China, 201800
[c]Zhejiang University, Department of Physics, Hangzhou, China, 310027
[d]Shanxi University, Collaborative Innovation Center of Extreme Optics, Taiyuan, China, 030006

Abstract. Entanglement serves as a fundamental resource for quantum information protocols, and hyperentanglement has received an explosively increasing amount of attention for its high-capacity characteristic. Increasing the scale of hyperentanglement, i.e., the number of modes in a hyperentangled system, is crucial for enhancing its capability in quantum information processing. Here we demonstrate the generation of large-scale continuous-variable (CV) hyperentanglement in three degrees of freedom (DOFs), including azimuthal and radial indexes of Laguerre-Gaussian (LG) modes and frequency. In our experiment, 216 pairs of hyperentangled modes are deterministically generated from the four-wave mixing process in an atomic vapor. Besides, we show that the entanglement between coherent LG superposition modes denoted by both azimuthal and radial quantum numbers can also be generated from this system. Such large-scale CV hyperentanglement in three DOFs presents an efficient scheme to significantly increase the information capacity of the CV system. Our results provide a new platform for studying CV quantum information and open the avenue for constructing high-capacity parallel and multiple-DOF CV quantum information protocols.

Keywords: hyperentanglement, multiplexing, orbital angular momentum, quantum optics, structured light.

*Address all correspondence to Jietai Jing, E-mail: jtjing@phy.ecnu.edu.cn

1 Introduction

Quantum entanglement, a form of strong correlation in quantum systems, is at the heart of quantum information science and technology.[?] Hyperentanglement, the simultaneous entanglement in more than one degree of freedom (DOF),[?,?] has attracted widespread attention and is a promising resource for implementing high-capacity quantum information protocols. There are two main branches of quantum information systems, namely discrete-variable (DV)[?] and continuous-variable (CV)[?] systems. The current trend is to combine them together to give full play to their respective advantages, establishing the so-called hybrid systems.[?,?,?] Our study here focuses on the CV system which has the advantage of deterministic generation of entanglement since all the generated

quantum states are fully taken into account without post-selection.[?] Compared with the well-developed DV hyperentanglement,[?,?,?,?,?,?,?,?,?] CV hyperentanglement[?,?] remains relatively unexplored. The scale of the hyperentanglement, i.e., the number of modes in a hyperentangled system, determines its capability of quantum information processing. However, it remains a challenge for CV hyperentanglement to scale to a large number of modes. Multiplexing, the indispensable concept of modern optical communication, can largely improve the information-carrying capacity by integrating multiple channels into one.[?,?,?,?] Multiplexing has also been transplanted to CV system by using different types of DOFs, including frequency,[?,?,?] time,[?,?,?] polarization,[?,?] and spatial mode.[?,?] By simultaneously multiplexing multiple DOFs, it is promising to develop large-scale CV hyperentanglement which can enable the implementation of high-capacity parallel and multiple-DOF CV quantum information protocols.

Laguerre-Gaussian (LG) modes, solution of the paraxial wave equation in cylindrical coordinates, are characterized by azimuthal index ℓ (an integer) and radial index p (a non-negative integer). These two quantum numbers provide two independent spatial DOFs. The azimuthal index ℓ, corresponding to the orbital angular momentum (OAM) of the optical field,[?,?] has been widely employed in an ocean of physical processes.[?,?,?,?,?,?,?,?,?,?,?,?,?] Meanwhile, OAM finds applications in both DV[?,?,?,?,?,?,?,?] and CV[?,?,?,?] quantum systems for the reason that it can form a high-dimensional Hilbert state space. In sharp contrast to the in-depth study of OAM, the radial index of the radial mode is often overlooked[?] and only attracts attention for the past few years.[?,?,?,?] Due to the self-healing properties of high-radial-index mode[?] and its propagation stability in graded-index fiber,[?] radial modes can find applications in practical long-distance communications for both free-space and fiber channels. More importantly, radial index provides another high-dimensional Hilbert state space for greatly boosting the information capacity of quantum systems in addition

to OAM. For example, high-dimensional DV entanglement[?,?] and high-dimensional DV quantum gates[?] have been demonstrated by considering both OAM and radial DOFs. However, such full consideration of the two quantum numbers or DOFs has not yet been demonstrated in the CV system. Combining such full consideration of OAM and radial DOFs with frequency DOF will enable the generation of large-scale CV hyperentanglement in three DOFs.

Here, we demonstrate the experimental generation of large-scale CV hyperentanglement in OAM, radial, and frequency DOFs. 216 pairs of hyperentangled modes defined by the discrete dimensions of these three DOFs are deterministically generated from the four-wave mixing (FWM) process in a hot ^{85}Rb atomic vapor. To the best of our knowledge, hyperentanglement has never been scaled to such a large number of modes in the CV quantum system. Moreover, we show that entangled coherent LG superposition modes with consideration of both azimuthal and radial quantum numbers can also be generated from this system. Such large-scale CV hyperentanglement in three DOFs largely enhances the data-carrying capacity of the CV system.

2 Principles and Methods

The FWM process is based on the double-Λ energy level configuration in the D1 line of ^{85}Rb. Pumped by a strong beam with a frequency of ω_{Pump}, this FWM process generates probe (conjugate) beam with a frequency of $\omega_{\mathrm{Pump}} - f$ ($\omega_{\mathrm{Pump}} + f$), where f denotes the frequency shifting from pump beam. Due to the OAM conservation and the phase-matching conditions of the FWM process, multitudinous pairs of $\mathrm{LG}^{\mathrm{Pr}}_{\ell,p,f}$ and $\mathrm{LG}^{\mathrm{Conj}}_{-\ell,p,-f}$ modes are generated simultaneously, where Pr and Conj indicate probe and conjugate beams, respectively. Labelling the creation operators of probe mode and conjugate mode as $\hat{a}^{\dagger}_{\ell,p,f}$ and $\hat{b}^{\dagger}_{-\ell,p,-f}$ respectively and denoting the interaction strength as the real parameter $\gamma_{\ell,p,f}$, the interaction Hamiltonian of the FWM process can be

written as

$$\hat{H} = \sum_{\ell,p,f} i\hbar\gamma_{\ell,p,f}\hat{a}^{\dagger}_{\ell,p,f}\hat{b}^{\dagger}_{-\ell,p,-f} + \mathrm{H.c.}, \tag{1}$$

where $\mathrm{H.c.}$ denotes the Hermitian conjugate. Then the corresponding time-evolution operator $U = e^{-i\hat{H}t/\hbar}$ is applied to vacuum state. The output field state can be expressed as the product of a series of two-mode squeezed vacuum states, i.e.,

$$|\psi\rangle_{out} = \prod_{\ell,p,f} |\psi\rangle_{\ell,p,f}, \tag{2}$$

where $|\psi\rangle_{\ell,p,f}$ is a squeezed vacuum state, or CV entangled state, of two modes with the opposite azimuthal quantum number, the same radial quantum number, and the opposite frequency shifting from pump beam. These orthogonal two-mode squeezed vacuum states are a series of CV entanglement in three independent DOFs, and each optical mode is defined by the discrete dimensions of all these three DOFs. In other words, the generated optical modes are simultaneously entangled in OAM, radial, and frequency DOFs, guaranteeing the generation of large-scale CV hyperentanglement (see Sec. S2 in the Supplementary Material for the detailed theoretical model). These three DOFs are equally important in generating CV hyperentanglement.

In our system, the physical quantities of entanglement are amplitude and phase quadratures, which have continuous spectrum, of the optical modes. Such CV entanglement manifests itself in strong correlation between the quantum fluctuations of quadratures of a pair of optical modes. For the purpose of verifying the existence of CV entanglement, the positivity under partial transposition (PPT) criterion[?] is used. One can determine if a state is entangled by constructing the covariance matrix σ from quadratures and calculating the smallest symplectic eigenvalue ν of the partially

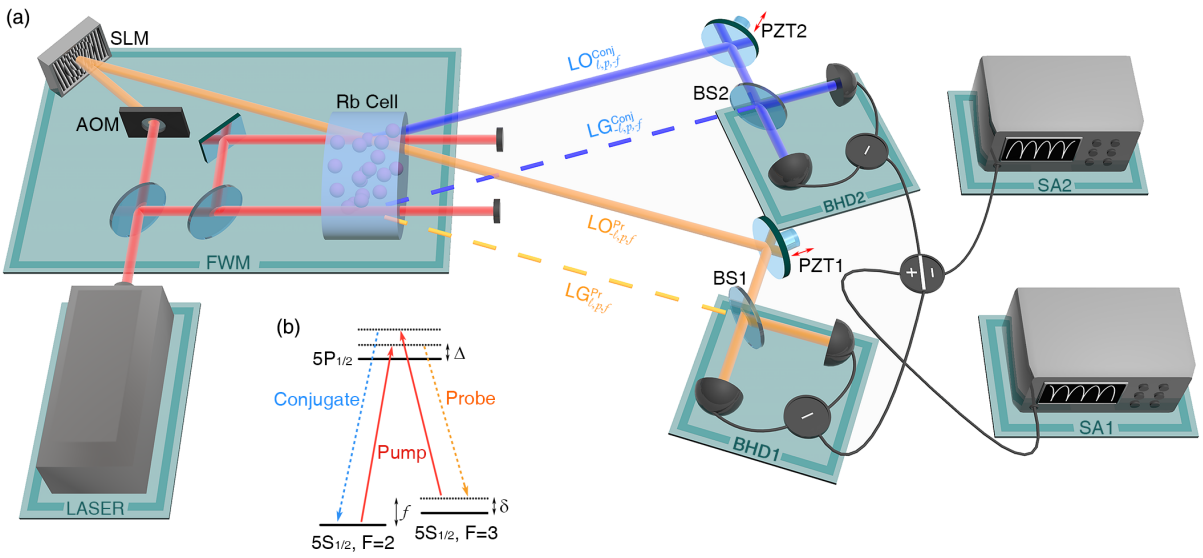

Fig 1 Experimental setup for generation and verification of large-scale CV hyperentanglement in three DOFs. (a) Two similar FWM processes happen in a ^{85}Rb vapor cell, one of which is seeded with probe beam modulated by an AOM and an SLM. The seeded FWM process generates the LOs of the two BHDs for extracting the desired modes generated from the unseeded FWM process. Two scanned PZTs are used to change the phases of the two BHDs for measuring the desired field quadrature. The photocurrents of the two BHDs are recorded by two SAs. AOM: acousto-optic modulator; BHD1 and BHD2: balanced homodyne detections; BS1 and BS2: 50:50 beam splitters; LO: local oscillator; PZT1 and PZT2: piezoelectric actuators; Rb cell: hot ^{85}Rb vapor cell; SA1 and SA2: spectrum analyzers; SLM: spatial light modulator. (b) The energy level diagram of the double-Λ configuration in the D1 line of ^{85}Rb. Δ: one-photon detuning; δ: two-photon detuning; f: frequency shifting from pump beam.

transposed covariance matrix. An entangled state is verified if ν is smaller than 1. Otherwise, the state is separable.

The detailed experimental setup is shown in Fig. 1(a), where a seeded and an unseeded FWM processes happen in the same ^{85}Rb vapor cell. The unseeded one is for generating large-scale CV hyperentanglement and the seeded one is for generating local oscillators (LOs) of the balanced homodyne detections (BHDs). A cavity stabilized Ti:sapphire laser produces a beam whose frequency is around 377.1102 THz (ω_{Pump}). The beam is divided into two, one of which is further split, serving as respective pump beams of the two FWM processes. The other beam is redshifted by f through an acousto-optic modulator (AOM) and then transformed into desired spatial modes by a spatial light modulator (SLM), serving as probe beam of the seeded FWM process. Strong

pump beams with a radius of 475 μm are focused at the center of the aforementioned ^{85}Rb vapor cell whose temperature is stabilized at 118 °C, and the probe and conjugate beams are symmetrically crossed with the pump beam at about 7 mrad. In order to measure the covariance matrix elements and verify the hyperentanglement from the unseeded FWM process, two BHDs are employed. One for detecting probe beam and the other one for detecting conjugate beam. Note that the generated fields will be projected onto $\mathrm{LG}_{\ell,p,f}$ mode if the LO carries $\mathrm{LG}_{-\ell,p,f}$ mode, which ensures the perfect extraction of the desired mode (see Sec. S3 in the Supplementary Material). In the experiment, extraction efficiency depends on the visibility of the BHD. The photocurrent from each BHD gives the variance of the single-beam quadrature while the two BHDs together with their photocurrent subtraction and addition give the covariance of the two-beam quadratures. Then these photocurrents are recorded by two spectrum analyzers (SAs) which are set to 300 kHz resolution bandwidth, 300 Hz video bandwidth, zero span, and 1.5 MHz center frequency. In this way, all the elements of the covariance matrix can be obtained.

3 Results

For demonstrating CV hyperentanglement in three DOFs, we perform measurements with varying ℓ, p, and f by changing the hologram displayed on SLM and the input radio-frequency signal of the AOM. The images of FWM output field for different modes are captured by a charge-coupled device (CCD) and shown in the upper panel of each subfigure of Fig. 2 where each subfigure stands for different frequency modes with $f = 3.04$ GHz [Fig. 2(a)], $f = 3.045$ GHz [Fig. 2(b)], and $f = 3.05$ GHz [Fig. 2(c)] as indicated by the lower panel. The intensity profiles from top to bottom in each image are amplified probe beam, pump beam, and newly generated conjugate beam respectively. It can be seen that the higher the LG mode order is, the bigger the beam size

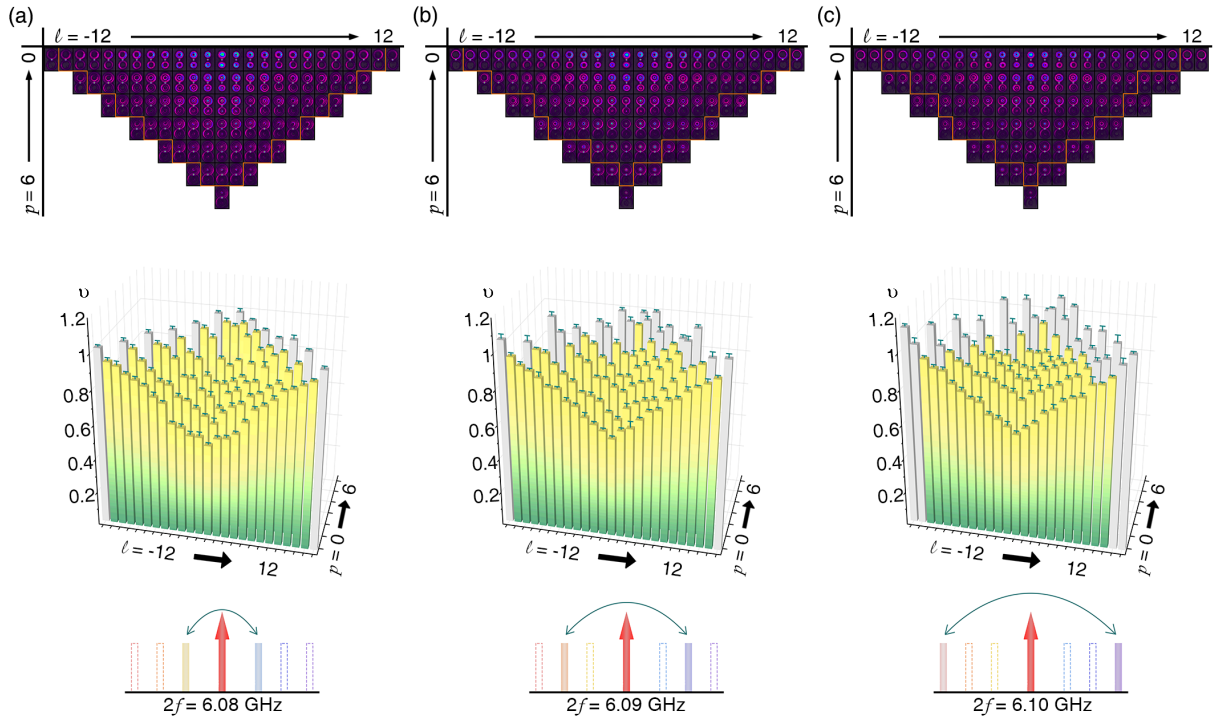

Fig 2 Experimental results for verifying large-scale CV hyperentanglement in three DOFs. 91 pairs of LG modes are measured at different frequency with (a) $f = 3.04$ GHz, (b) $f = 3.045$ GHz, and (c) $f = 3.05$ GHz. The upper panel of each subfigure shows the CCD captured images of LG modes generated from the FWM process with varying both quantum numbers of azimuthal index ℓ and radial index p. Labeled columns represent the azimuthal index ℓ of the probe beam, while labeled rows represent the radial index p of the probe beam. The entangled LG modes are enclosed inside the orange frame. The middle panel of each subfigure shows the smallest symplectic eigenvalue ν of the partially transposed covariance matrix as a function of the two quantum numbers ℓ and p, respectively. The lower panel of each subfigure indicates the frequency of hyperentangled LG modes.

will be. Such increment in beam size results in the reduced overlap with the pump beam and thus weaker nonlinear interaction strength, leading to smaller intensity gain. And the smallest symplectic eigenvalues ν of the partially transposed covariance matrices for the different modes are shown in the middle panel of each subfigure of Fig. 2. As can be seen, with the LG mode order getting higher, the value of ν increases due to the decreasing of nonlinear interaction strength, indicating the weakening of the entanglement degree. For high-order LG modes, ν being not smaller than 1 indicates the vanishment of the CV entanglement. It can also be found that the larger the value of radial index p is, the narrower the azimuthal index range of the OAM modes possessing entanglement will be. For example, as shown in Fig. 2(a), when $f = 3.04$ GHz, for radial index $p = 4$, only the OAM modes with azimuthal index ℓ from -3 to 3 possess entanglement, while for radial index $p = 0$, the range of azimuthal index ℓ of OAM modes possessing entanglement is from -11 to 11. The mutual restriction of these two quantum numbers in terms of entanglement generation is due to the fact that the increase of either one of these two quantum numbers can lead to an increase in beam size. In addition, the symplectic eigenvalue ν for OAM entanglement in the case of radial index $p = 0$ is smaller than the corresponding value with a nonzero radial index, which shows that the quality of hyperentanglement in OAM and radial DOFs is less than the quality of entanglement in OAM DOF. Nevertheless, under our experimental condition, for maintaining entanglement, the maximal range of ℓ is from -11 to 11 while the maximal range of p is from 0 to 5. Figure 2(a) gives the results of hyperentanglement in OAM and radial DOFs with the generation of 78 pairs of LG modes when $f = 3.04$ GHz. In order to realize CV hyperentanglement in three DOFs, we utilize the frequency mode by changing the amount of frequency shifting f and repeating the above measurements. Similar results for $f = 3.045$ GHz and $f = 3.05$ GHz are shown in Figs. 2(b) and 2(c), respectively. Altogether, 216 pairs of hyperentangled modes in OAM, radial, and frequency

DOFs are deterministically generated. For a fixed frequency, the possible number of pairs of entangled spatial modes possibly created by this system in the ideal case is estimated to be around 297 according to the Schmidt number[?,?,?] which is roughly the number of modes pairs coupled in the gain region (see Sec. S8 in the Supplementary Material). However, various experimental imperfections are unavoidable, such as atomic absorption, propagation losses, imperfect homodyne visibilities, non-unity quantum efficiency of photodiode, and scattered pump light, which introduce excess noise and deteriorate the entanglement. Therefore, the number of experimentally accessible entangled spatial mode pairs is lower than the theoretically predicted Schmidt number. Taking into account experimental parameters and these aforementioned experimental imperfections, the theoretical predictions of the smallest symplectic eigenvalue ν agree well with the corresponding experimental results, and the fidelities between the theoretically predicted and experimentally generated hyperentangled states are all above 0.9 (see Sec. S8 in the Supplementary Material).

Going a step further, it is interesting to investigate the entanglement properties of coherent LG superposition modes by considering both quantum numbers ℓ and p, which shows the potential advantage of our system for demonstrating parallel quantum information processing. Here we fix f at 3.04 GHz. Firstly, the LOs are tailored by seeding $\mathrm{LG}_{-1,3}$+$\mathrm{LG}_{2,1}$ mode into the FWM process [see Fig. 3(a) for the theoretical intensity profile and phase pattern and Fig. 3(b) for the experimentally observed intensity profile], and the covariance matrix of $\mathrm{LG}^{\mathrm{Pr}}_{-1,3} + \mathrm{LG}^{\mathrm{Pr}}_{2,1}$ and $\mathrm{LG}^{\mathrm{Conj}}_{1,3} + \mathrm{LG}^{\mathrm{Conj}}_{-2,1}$ modes can be measured. The smallest symplectic eigenvalue ν is calculated to be 0.691 ± 0.013, indicating the existence of entanglement between these two LG superposition modes. Secondly, we turn to study another type of coherent LG superposition mode $\mathrm{LG}_{\ell,p}$±$\mathrm{LG}_{-\ell,p}$. The intensity profile of this sort of mode is constituted of $p + 1$ radial circles and 2ℓ angularly symmetric petals in each radial circle as shown in Figs. 3(c) and 3(d), making it useful for free-

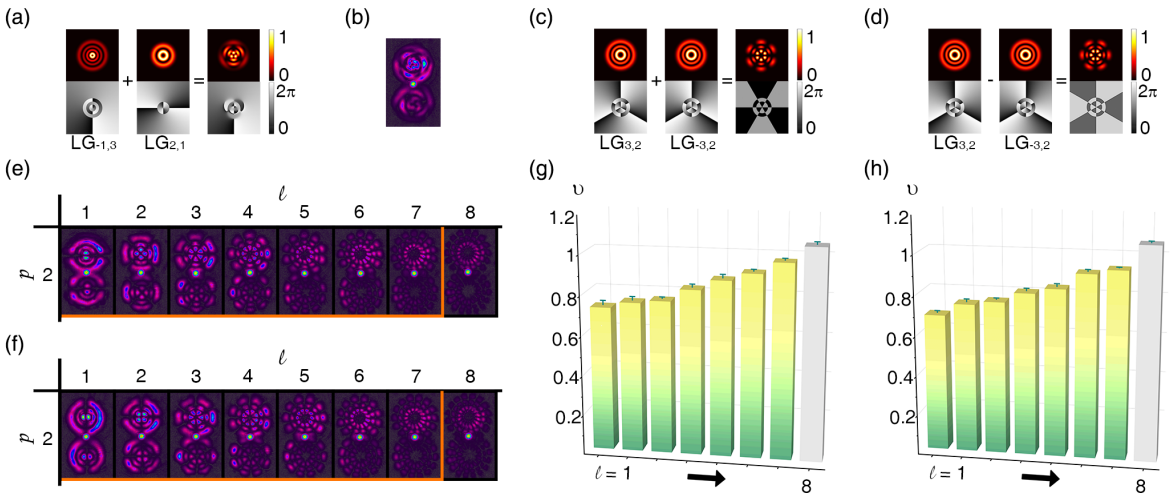

Fig 3 Experimental results for verifying CV entanglement between coherent LG superposition modes with considering both azimuthal and radial quantum numbers in the case of f = 3.04GHz. (a) The theoretical intensity profile (top row) and phase pattern (bottom row) of $\mathrm{LG}_{-1,3}+\mathrm{LG}_{2,1}$ mode. (b) The CCD captured image of entangled $\mathrm{LG}^{\mathrm{Pr}}_{-1,3}+\mathrm{LG}^{\mathrm{Pr}}_{2,1}$ mode and $\mathrm{LG}^{\mathrm{Conj}}_{1,3}+\mathrm{LG}^{\mathrm{Conj}}_{-2,1}$ mode. (c) [(d)] The theoretical intensity profile and phase pattern of $\mathrm{LG}_{3,2}+\mathrm{LG}_{-3,2}$ [$\mathrm{LG}_{3,2}-\mathrm{LG}_{-3,2}$] mode. (e) [(f)] The CCD captured images of $\mathrm{LG}^{\mathrm{Pr}}_{\ell,2}+\mathrm{LG}^{\mathrm{Pr}}_{-\ell,2}$ [$\mathrm{LG}^{\mathrm{Pr}}_{\ell,2}-\mathrm{LG}^{\mathrm{Pr}}_{-\ell,2}$] mode and $\mathrm{LG}^{\mathrm{Conj}}_{-\ell,2}+\mathrm{LG}^{\mathrm{Conj}}_{\ell,2}$ [$\mathrm{LG}^{\mathrm{Conj}}_{-\ell,2}-\mathrm{LG}^{\mathrm{Conj}}_{\ell,2}$] mode for ℓ varying from 1 to 8. The entangled modes are enclosed inside the orange frame. (g) [(h)] The measured smallest symplectic eigenvalue ν as a function of ℓ for $\mathrm{LG}^{\mathrm{Pr}}_{\ell,2}+\mathrm{LG}^{\mathrm{Pr}}_{-\ell,2}$ [$\mathrm{LG}^{\mathrm{Pr}}_{\ell,2}-\mathrm{LG}^{\mathrm{Pr}}_{-\ell,2}$] and $\mathrm{LG}^{\mathrm{Conj}}_{-\ell,2}+\mathrm{LG}^{\mathrm{Conj}}_{\ell,2}$ [$\mathrm{LG}^{\mathrm{Conj}}_{-\ell,2}-\mathrm{LG}^{\mathrm{Conj}}_{\ell,2}$] modes.

space communication under turbulent conditions.[?] Specifically, we investigate the entanglement between $\mathrm{LG}^{\mathrm{Pr}}_{\ell,2}+\mathrm{LG}^{\mathrm{Pr}}_{-\ell,2}$ [$\mathrm{LG}^{\mathrm{Pr}}_{\ell,2}-\mathrm{LG}^{\mathrm{Pr}}_{-\ell,2}$] and $\mathrm{LG}^{\mathrm{Conj}}_{-\ell,2}+\mathrm{LG}^{\mathrm{Conj}}_{\ell,2}$ [$\mathrm{LG}^{\mathrm{Conj}}_{-\ell,2}-\mathrm{LG}^{\mathrm{Conj}}_{\ell,2}$] modes with ℓ from 1 to 8, and the corresponding FWM output images and smallest symplectic eigenvalues ν are shown in Fig. 3(e) [Fig. 3(f)] and Fig. 3(g) [Fig. 3(h)], respectively. With the increase of azimuthal index ℓ, the beam size gets bigger, resulting in weaker nonlinear interaction strength. As a consequence, the intensity gain decreases, and ν increases. For ℓ in the range from 1 to 7, these coherent LG superposition modes maintain entangled. These experimental results are consistent with the ones in Fig. 2 and clearly verify the entanglement between coherent LG superposition modes with both azimuthal and radial quantum numbers involved.

4 Conclusions and Discussion

In summary, we have experimentally implemented large-scale CV hyperentanglement in three DOFs. 216 pairs of hyperentangled modes in OAM (ℓ), radial (p), and frequency (f) DOFs are generated from the FWM process in a single hot ^{85}Rb vapor cell. In addition, we demonstrate the entanglement of coherent LG superposition modes denoted by both azimuthal and radial quantum numbers. Such large-scale CV hyperentanglement greatly enhances the information-carrying capacity of the CV system. Several beneficial improvements can be adopted to further enlarge the number of entangled mode pairs, such as decreasing the cell length,[?] increasing the pump beam size,[?] tailoring the pump beam profile,[?] and exploiting more DOFs. Although we have only chosen three frequency sidebands to realize multiplexing, the actual frequency bandwidth for maintaining entanglement is at the level of tens of MHz (see Sec. S5 in the Supplementary Material), which is determined by the atomic system itself. In order to substantially improve the frequency bandwidth for maintaining entanglement, one possibility is to replace the atomic medium with nonlinear crystal such as PPLN waveguide.[?]

Utilizing LG mode sorter[?,?] and frequency filter cavity,[?] these hypergenerated modes can be efficiently spatially separated (see Sec. S9 in the Supplementary Material), making our scheme particularly useful for constructing high-capacity parallel and multiple-DOF quantum communication protocols. In parallel quantum communication,[?,?] multiple quantum communication channels can be constructed without the crosstalk from each other, and various quantum information tasks[?,?,?] can be performed simultaneously, which significantly enhances the information capacity and diversity of quantum communication systems. Besides, a complex quantum system cannot be fully described by a single DOF, and a critical issue that must be addressed is how to teleport more

than one DOF simultaneously. In this respect, quantum teleportation of multiple DOFs of a single photon has been demonstrated in DV system using the hyperentanglement in both spin angular momentum and OAM.[?] Such multiple-DOF quantum teleportation in CV system, whose realization requires the generation of CV hyperentanglement, has never been reported. Our large-scale CV hyperentanglement provides the possibility to realize such multiple-DOF quantum teleportation in CV system, even more generally, multiple-DOF quantum communication protocols.

Disclosures

The authors declare no conflicts of interest.

Acknowledgments

We acknowledge the useful discussions with Xiaozhou Pan and Lixiang Chen. This work was funded by Innovation Program of Shanghai Municipal Education Commission (Grant No. 2021-01-07-00-08-E00100); the National Natural Science Foundation of China (11874155, 91436211, 11374104, 12174110); Basic Research Project of Shanghai Science and Technology Commission (20JC1416100); Natural Science Foundation of Shanghai (17ZR1442900); Minhang Leading Talents (201971); Program of Scientific and Technological Innovation of Shanghai (17JC1400401); Shanghai Sailing Program (21YF1410800); National Basic Research Program of China (2016YFA0302103); Shanghai Municipal Science and Technology Major Project (2019SHZDZX01); the 111 project (B12024).

Data, Materials, and Code Availability

The data that support the results within this paper and other findings of the study are available from the corresponding author upon reasonable request.

List of Figures

2 Experimental results for verifying large-scale CV hyperentanglement in three DOFs. 91 pairs of LG modes are measured at different frequency with (a) $f = 3.04$ GHz, (b) $f = 3.045$ GHz, and (c) $f = 3.05$ GHz. The upper panel of each subfigure shows the CCD captured images of LG modes generated from the FWM process with varying both quantum numbers of azimuthal index ℓ and radial index p. Labeled columns represent the azimuthal index ℓ of the probe beam, while labeled rows represent the radial index p of the probe beam. The entangled LG modes are enclosed inside the orange frame. The middle panel of each subfigure shows the smallest symplectic eigenvalue ν of the partially transposed covariance matrix as a function of the two quantum numbers ℓ and p, respectively. The lower panel of each subfigure indicates the frequency of hyperentangled LG modes.

3 Experimental results for verifying CV entanglement between coherent LG superposition modes with considering both azimuthal and radial quantum numbers in the case of f = 3.04GHz. (a) The theoretical intensity profile (top row) and phase pattern (bottom row) of $\mathrm{LG}_{-1,3} + \mathrm{LG}_{2,1}$ mode. (b) The CCD captured image of entangled $\mathrm{LG}^{\mathrm{Pr}}_{-1,3} + \mathrm{LG}^{\mathrm{Pr}}_{2,1}$ mode and $\mathrm{LG}^{\mathrm{Conj}}_{1,3} + \mathrm{LG}^{\mathrm{Conj}}_{-2,1}$ mode. (c) [(d)] The theoretical intensity profile and phase pattern of $\mathrm{LG}_{3,2} + \mathrm{LG}_{-3,2}$ [$\mathrm{LG}_{3,2} - \mathrm{LG}_{-3,2}$] mode. (e) [(f)] The CCD captured images of $\mathrm{LG}^{\mathrm{Pr}}_{\ell,2} + \mathrm{LG}^{\mathrm{Pr}}_{-\ell,2}$ [$\mathrm{LG}^{\mathrm{Pr}}_{\ell,2} - \mathrm{LG}^{\mathrm{Pr}}_{-\ell,2}$] mode and $\mathrm{LG}^{\mathrm{Conj}}_{-\ell,2} + \mathrm{LG}^{\mathrm{Conj}}_{\ell,2}$ [$\mathrm{LG}^{\mathrm{Conj}}_{-\ell,2} - \mathrm{LG}^{\mathrm{Conj}}_{\ell,2}$] mode for ℓ varying from 1 to 8. The entangled modes are enclosed inside the orange frame. (g) [(h)] The measured smallest symplectic eigenvalue ν as a function of ℓ for $\mathrm{LG}^{\mathrm{Pr}}_{\ell,2} + \mathrm{LG}^{\mathrm{Pr}}_{-\ell,2}$ [$\mathrm{LG}^{\mathrm{Pr}}_{\ell,2} - \mathrm{LG}^{\mathrm{Pr}}_{-\ell,2}$] and $\mathrm{LG}^{\mathrm{Conj}}_{-\ell,2} + \mathrm{LG}^{\mathrm{Conj}}_{\ell,2}$ [$\mathrm{LG}^{\mathrm{Conj}}_{-\ell,2} - \mathrm{LG}^{\mathrm{Conj}}_{\ell,2}$] modes.